Characterization of the Yeast Peroxiredoxin Ahp1 in Its Reduced Active and Overoxidized Inactive Forms Using NMR†

Xavier Trivelli,‡ Isabelle Krimm,*,‡ Christine Ebel,§ Lionel Verdoucq,|| Valérie Prouzet-Mauléon,⊥ Yvette Chartier,|| Pascale Tsan,‡ Guy Lauquin,⊥ Yves Meyer,|| and Jean-Marc Lancelin*,‡

Laboratoire de RMN Biomoléculaire associé au CNRS, Université Claude Bernard−Lyon 1, Ecole Supérieure de Chimie Physique Electronique de Lyon, 69622 Villeurbanne, Laboratoire de Physiologie Végétale associé au CNRS, Université de Perpignan, 66860 Perpignan, Laboratoire de Biophysique Moléculaire, Institut de Biologie Structurale Jean-Pierre Ebel (CEA-CNRS-UJF), 38027 Grenoble, and Laboratoire de Physiologie Moléculaire et Cellulaire, Institut de Biochimie et Génétique Cellulaires associé au CNRS, Université Bordeaux 2, 33077 Bordeaux, France

Received August 29, 2003; Revised Manuscript Received October 2, 2003

ABSTRACT: Peroxiredoxins (Prx's) are a superfamily of thiol-specific antioxidant proteins present in all organisms and involved in the hydroperoxide detoxification of the cell. The catalytic cysteine of Prx's reduces hydroperoxides and is transformed into a transient sulfenic acid (Cys-SOH). At high hydroperoxide concentration, the sulfenic acid can be overoxidized into a sulfinate, or even a sulfonate. We present here the first peroxiredoxin characterization by solution NMR of the *Saccharomyces cerevisiae* alkylhydroperoxide reductase (Ahp1) in its reduced and in vitro overoxidized forms. NMR ^{15}N relaxation data and ultracentrifugation experiments indicate that the protein behaves principally as a homodimer (2×19 kDa) in solution, regardless of the redox state. In vitro treatment of Ahp1 by a large excess of *t*BuOOH leads to an inactive form, with the catalytic cysteine overoxidized into sulfonate, as demonstrated by ^{13}C NMR. Depending on the amino acid sequence of their active site, Prx's are classified into five different families. In this classification, Ahp1 is a member of the scarcely studied D-type Prx's. Ahp1 is unique among the D-type Prx's in its ability to form an intermolecular disulfide. The peptidic sequence of Ahp1 was analyzed and compared to other D-type Prx sequences.

In 1998−1999 three research groups independently identified a new antioxidant protein in the yeast *Saccharomyces cerevisiae*. The first group noticed a new protein with a glutamine synthase protection activity different from that of the first yeast peroxiredoxin characterized, and named it type-II thiol peroxidase (TPx) (*1*). The second group found that the alkyl hydroperoxide reductase gene (Ahp1) increases tolerance to *t*BuOOH of transcriptional regulator *skn7* null mutant (*2*). The third group isolated the theoretical product of the genomic ORF YLR109W as a novel thioredoxin target (*3*). This new antioxidant protein, also referred to as thiol-specific antioxidant II (TSA II) or third cytosolic TPx (cTPx III) (*4*), will be named Ahp1 in this text. Ahp1 is a cytosolic protein of 176 residues whose production can be induced in yeast by oxygen and hydroperoxides (*4*). Its catalytic efficiency (V_{max}/K_{max}) with H_2O_2 as a substrate is approximately 1/14 compared to the efficiency with cumene hydroperoxide as a substrate (*1*). Ahp1 has been also shown to act as an important cytoplasmic thioredoxin-linked alkyl hydroperoxide peroxidase in the stationary phase of the yeast (*4*).

Peroxiredoxins (Prx's)[1] are a superfamily of thiol-specific antioxidant proteins, also known as thioredoxin peroxidase or alkyl hydroperoxidase reductase with essential protective properties against hydrogen peroxide, organic hydroperoxide, and peroxynitrite (*5*). Some eukaryotic Prx's are also found to be regulators of H_2O_2-mediated signal transduction (*6*, *7*). Prx's are abundant in yeast, plant, and animal cells and in most eubacteria and archaea, and exist in several isoforms in all these organisms. Prx's contain a completely conserved N-terminal catalytic cysteine called the *peroxidatic* cysteine (Cys62-S_PH in Ahp1). According to the occurrence of a second conserved cysteine or not, the Prx's are divided into two groups, the 1-Cys and 2-Cys Prx's. The peroxidatic cysteine attacks the hydroperoxide ROOH and is oxidized into a sulfenic acid, Cys-S_POH, while alcohol ROH is released. Three mechanistic classes (the 1-Cys, 2-Cys, and atypical 2-Cys Prx's) are distinguished according to the next enzymatic step as illustrated in Figure 1. The 1-Cys Prx peroxidatic cysteine is oxidized into a stable sulfenic acid, Cys-S_POH, and regenerated by an unknown reducing agent (*8*) (Figure 1, I). The 2-Cys Prx's have a second conserved cysteine located in the C-terminus (Figure 1, II). This C-terminal *resolving* cysteine Cys-S_RH attacks the sulfenic

† This work was supported by grants from CNRS (Program PCV99-00, GDR "Thiorédox" 2477, UMR 5078-5180) and financial support from the French Ministère de l'Education Nationale, de la Recherche et des Technologies, to X.T., I.K., and L.V. and from Région Aquitaine to V.P.-M.

* To whom correspondence should be addressed. Phone/Fax: (+33) 4 72 43 13 95 (J.-M.L.). E-mail: lancelin@hikari.cpe.fr (J.-M.L.).

‡ Université Claude Bernard−Lyon 1.

§ Institut de Biologie Structurale Jean-Pierre Ebel.

|| Université de Perpignan.

⊥ Université Bordeaux 2.

[1] Abbreviations: DTT, dithiothreitol; HSQC, heteronuclear single-quantum coherence; NMR, nuclear magnetic resonance; NOE, nuclear Overhauser effect; NOESY, NOE spectroscopy; PDB, Protein Data Bank; Prx, peroxiredoxin; R_1, longitudinal relaxation rate; R_2, transversal relaxation rate; ROOH, hydroperoxide; SDS−PAGE, sodium dodecyl sulfate−polyacrylamide gel electrophoresis; *t*BuOOH, *tert*-butyl hydroperoxide; Trx, thioredoxin.

10.1021/bi035551r CCC: $25.00
Published on Web 11/11/2003

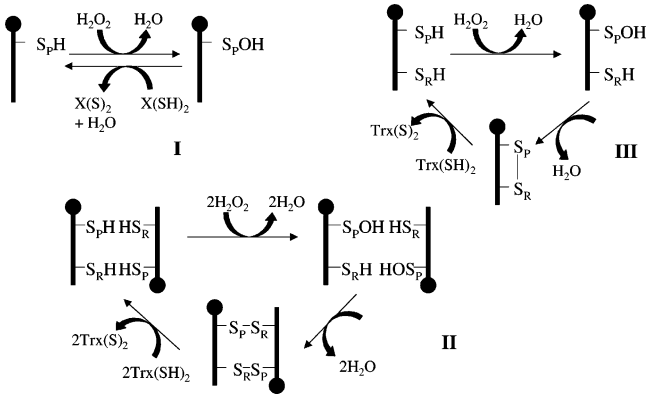

FIGURE 1: Schematic representation of the catalytic mechanism of (I) 1-Cys, (II) 2-Cys and (III) atypical 2-Cys Prx's. S_PH corresponds to the peroxidatic cysteine of the active site and $X(SH)_2$ to the unknown reducer of 1-Cys Prx. Trx is the thioredoxin system that reduces the 2-Cys and some atypical 2-Cys Prx's.

acid Cys-S_POH of another monomer to form an intermolecular disulfide bridge. In the case of the atypical 2-Cys Prx's (Figure 1, III), the resolving cysteine Cys-S_RH attacks the sulfenic acid Cys-S_POH of the same monomer and an intramolecular disulfide bridge is formed (*9*). The 2-Cys and atypical 2-Cys Prx's are known to be regenerated by thiol reducers such as thioredoxins.

Prx's can also be classified according to their sequence homology (*3*, *10*, *11*). More precisely, on the basis of the conserved residues around the active site, five subfamilies that we will name A-, B-, C-, D-, and E-type Prx's can be identified (Figure 2). A-type Prx's (A-labeled proteins in Figure 2) contain a second conserved cysteine localized in the last 30 C-terminal residues within a VCP pattern. All A-type Prx's are 2-Cys Prx's. The second subfamily comprises most of the 1-Cys Prx's (B in Figure 2). The third subfamily (C-type Prx's, C in Figure 2) includes the bacterioferritin comigratory proteins and the PrxQ's (*12*). C-type Prx's form an intramolecular disulfide bridge between the unusual motif CxxxxC. The fourth subfamily (D-type Prx's, D in Figure 2) contains about 60 Prx's homologous to Ahp1 (Figure 3). The last subfamily (E-type Prx's, E in Figure 2) contains a conserved resolving cysteine located about 40 residues after the peroxidatic one, conferring E-type Prx's atypical 2-Cys properties (*13*). The D-type differs from the other types in its strong functional heterogeneity. From a mechanistic point of view, D-type Prx's behave like atypical 2-Cys Prx's (mammalian PrxV (*9*)), 1-Cys Prx's (bacterial or plant Prx (*14*)), or 2-Cys Prx's (yeast Ahp1 (*1*, *3*)).

All Prx's characterized so far have been found to be homodimers or larger species (*5*). The oligomerization of A-type Prx's has been shown to be redox-linked, which could regulate the Prx enzymatic and signaling activities (*5*). The oligomerization state of other Prx's and its functional meaning are poorly understood. Recently, the E-type thiol peroxidase from *Escherichia coli* was found to be dimeric, independent of its redox state. However, this dimerization might be peculiar, since it is not apparently required for the catalytic reaction (*15*).

I

```
                 50        60        70        80        90       100       110       120       130       140
                 ....|.....|.....|.....|.....|.....|.....|.....|.....|.....|.....|.....|.....|.....|....
A.hPrxII   …KYVVLFFYPLDFTFVCP-TEIIAFSNRAEDFR--KLGCEVLGVSVDSQFTHLAWINTPRK---EGGLGPLNIPLLADVTRR-LSEDYGVLKTDEGIA--------YRGLF…197
  rPrxI    …KYVVFFFYPLDFTFVCP-TEIIAFSDRAEEFK--KLNCQVIGASVDSHFSHLAWINTPKK---QGGLGPMNIPLVSDPKRT-IAQDYGVLKADEGIS--------FRGLF…199
  TryP     …KYVVLFFYPMDFTFVCP-TEIIQFSDDAKRFA--EINTEVISCSCDSEYSHLQWTSVDRK---KGGLGPMAIPMLADKTKA-IARAYGVLDEDSGVA--------YRGVF…188
  AhpC     …RWSVFFFYPADFTFVCP-TELGDVADHYEELQ--KLGVDVYSVSTDTHFTHKAWHSSSE------TIAKIKYAMIGDPTGA-LTRNFDNMREDEGLA--------DRATF…186
B.hPrxVI   …SWGILFSHPRDFTPVCT-TELGRAAKLAPEFA--KRNVKLIALSIDSVEDHLAWSKDINAYNSEEPTEKLPFPIIDDRNRE-LAILLGMLDPAEKD--EKGMPVTARVVF…224
  ymTpx    …SWGVLFSHPADFTPVCT-TEVSAFAKLKPEFD--KRNVKLIGLSVEDVESHEKWIQDIK---EIAKVKNVGFPIIGDTFRN-VAFLYDMVDAEGFKNINDGSLKTVRSVF…215
C.slPrxQ   …KPVVVYFYPADETPGGT-KQACAFRDSYEKFK--KAGAEVVGISGDSSESHKAFAKKYK----------LPFTLLSDEGNK-VRKEWGVPSDLFGTL-------PGRETY…186
  yPrxQ    …RVVVFFVYPRASTPGGT-RQACGFRDNYQELK--K-YAAVFGLSADSVTSQKKFQSKQN----------LPYHLLSDPKRE-FIGLLGAKKTPLSGS--------IRSHF…215
D.hPrxV    …KKGVLFGVPGAFTPGGSKTHLPGFVEQAEALK-AKGVQVVACLSVNDAFVTGEWGRATKAEG--------KVRLLADPTGA-FGKETDLLLDDSLVSIF-GNRRLKRFSM…161
  pPrx     …KKVILFGVPGAFTPTCSLKHVPGFIEKAGELK-SKGVTEILCISVNDPFVMKAWAKSYPENK--------HVKFLAD--GS-ATYTHALGLELDLQGKG-LGTRSRRFAL…162
  HybrP    …KTVIVFSLPGAFTPTCSSSHLPRYNELAPVFK-KYGVDDILVVSVNDTFVMNAWKEDEKSE---------NISFIPDGNGE-FTEGMGMLVGKEDLG---FGKRSWRYSM…241
  Ahp1     …KKVIITGAPAAFSPTCTVSHIPGYINYLDELVKEKEVDQVIVVTVDNPFANQAWAKSLGVKD------TTHIKFASDPGGA-FTKSIGFELAVGD-G----VYWSGRWAM…176
E.EcTPx    …KRKVLNIFPSIDTGVCA-ASVRKFNQLATEI----DNTVVLCISADLPFAQSRFCGAEGLN---------NVITLSTFRNAEFLQAYGVAIA-DGPL----KGLAARAVV…167
  BsTPx    …KVTIISVIPSIDTGVCD-AQTRRFNEEAAKL----GDVNVYTISADLPFAQARWCGANGID---------KVETLSDHRDMSFGEAFGVYIK-EL-------RLLARSVF…166
```

II

```
A    YPxDF[T/S]FVCPP[T/S]E[I/L/V]
B    HPxDFTPVCPTTE[L/F]
C    YPx[A/D]xTP[G/V]CPTx[Q/E]xCx[F/L]
D    xP[G/A]A[F/Y][T/S][P/G]xCP[S/T]xxHxP
E    xP[D/S]DTxVCPxx[Q/S]x[K/R]
```

FIGURE 2: (I) Partial sequence alignment of peroxiredoxins. A-, B-, C-, D-, and E-labeled proteins are A-, B-, C-, D-, and E-type Prx's, respectively (see the text). The alignment shows the region where the maximum of homology is found. The numbering corresponds to the sequence of Ahp1. Bold characters indicate conserved amino acids discussed in the text, and the boxed area highlights the residues of the active site. Peroxidatic and resolving cysteines are shown in black boxes. hPrx II is the human Prx II, rPrxI is the rat PrxI, TryP is the *Crithidia fasciculata* tryparedoxin peroxidase, AhpC is the *Salmonella typhimurium* alkyl hydroperoxide reductase peroxidase component, hPrxVI is the human PrxVI, ymTPx is the *S. cerevisiae* mitochondrial Prx, slPrxQ is the *Sedum lineare* PrxQ, yPrxQ is the *S. cerevisiae* nuclear Prx, hPrxV is the human PrxV, pPrx is the phloem poplar Prx, and HybrP is the *Haemophilus influenzae* hybrid Prx5. Crystallographic structures (PDB code) have been resolved for hPrxII (1QMV (*41*)), rPrxI (1QQ2 (*43*)), TryP (1E2Y (*45*)), AhpC (1KYG, 1N8J (*6*, *40*)), hPrxVI (1PRX (*8*)), hPrxV (1HD2, 1H4O (*42*)), and HybrP (1NM3 (*34*)). (II) Consensus sequences of the active site of A-, B-, C-, D-, and E-type Prx's. The consensus sequences have been defined from 189, 72, 50, 60, and 50 peptidic sequences from the Swiss-Prot database, respectively.

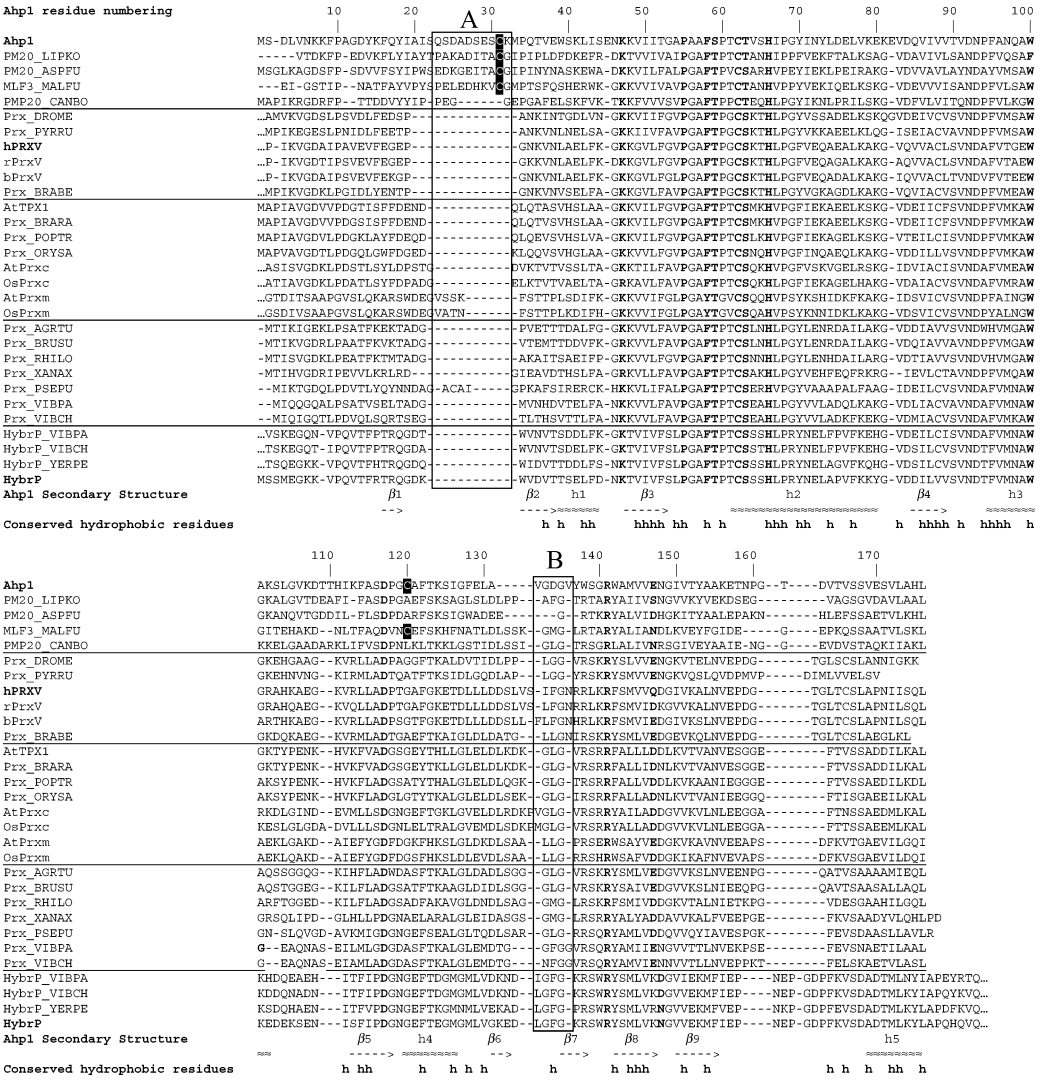

FIGURE 3: Partial sequence alignment of D-type peroxiredoxins. The alignment shows the region where the maximum of homology is found. Only 30 of the 60 D-type Prx sequences are shown. The numbering corresponds to the sequence of Ahp1. Eleven residues strictly or nearly strictly conserved in D-type Prx's are displayed in bold (see the text). Nonperoxidatic cysteines in fungus Prx's are indicated in black boxes. Boxes A and B highlight two loops in Ahp1 discussed in the text, and the gray boxes show residues conserved in all D-type Prx's but Ahp1. Residues with conserved hydrophobic character are indicated by "h" in the bottom line. Human PrxV (hPrxV) and *H. influenzae* hybrid Prx5 (HybrP) whose structures have been solved are indicated in bold. From the top to the bottom, lines distinguish fungus, animal, plant, and bacterium Prx's and bacterial hybrid Prx5. In the N-terminus, putative targeting sequences are found for 16 proteins (Supporting Information Table S2). More details of the 30 peptidic sequences (number of residues, organism, short classification, SwissProt or Tr-EMBL access code) are found in the Supporting Information (Table S2).

Recently, it was shown that Prx's exposed to a high concentration of hydroperoxide are inactivated in vitro and in vivo (*6*, *7*, *16*). This inactivation is caused by the overoxidation of the peroxidatic cysteine into a sulfinate/sulfonate ($Cys\text{-}SO_2^-/SO_3^-$). Prouzet and co-workers have identified a modified form of Ahp1 in *S. cerevisiae sod1* and *lys7* null mutants without superoxide dismutase activity (*17*). As evident from two-dimensional gel electrophoresis, the modified form has a molecular weight similar to that of the wild-type protein but presents a more acidic isoelectric point (4.44 vs 4.56). The modified protein is monomeric on nonreducing SDS−PAGE, unlike active Ahp1, and is inefficient in reducing *t*BuOOH. The properties of this modified Ahp1 are consistent with an overoxidized peroxidatic cysteine.

We report here the first NMR study of a member of the peroxiredoxin superfamily. Ahp1 is a member of the D-type Prx's and is unique among the D-type in its ability to form an intermolecular disulfide (*1*, *3*). This is due to the occurrence of a resolving cysteine at position 120. This cysteine is not conserved in other Prx's (Figure 3), except in yeast *Mallassezia furfur* (*18*). The assignment of the backbone nuclei enabled us to define the topology of Ahp1. The oligomerization state of Ahp1 was determined by analysis of ^{15}N relaxation data and analytical ultracentrifugation. We have characterized and defined by NMR the overoxidized inactive form of Ahp1. An analysis of the amino acid sequences of the D-type Prx's is presented. This NMR study will be the basis of further work concerning structural and dynamical properties of Prx's in solution, which will complement the X-ray studies undertaken to date.

EXPERIMENTAL PROCEDURES

Sample Preparation. The PCR product of Ahp1 was cloned into the plasmid pMosBlue (Amersham Life Science), and introduced into *E. coli* strain DH5α. Plasmid pET16b (Novagen) was used to express recombinant protein in *E.*

coli BL21(DE3). Manipulations of DNA and *E. coli* were as previously described (*3*). BL21(DE3) bacteria containing pET16b-Ahp1 were grown in 10 mL of unlabeled LB medium and then transferred into 150 mL and later into 1.5 L of labeled M9 medium. Labeled M9 medium contained 1 g·L^{-1} $^{15}NH_4Cl$, 4 g·L^{-1} [$^{13}C_6$]-D-glucose and 75/25 v/v D_2O/H_2O according to the protein labeling. When OD_{600} reached 0.5, recombinant protein expression was induced by addition of 1 mM isopropyl 1-thio-β-D-galactopyranoside for 2.5 h at 37 °C. Cells were pelleted and stored at −80 °C for the subsequent protein extraction and broken by a hydraulic press (Carver, model 3968) at 3500 psi and −80 °C. Broken cells were then resuspended in 10 mL of chilled 1× binding buffer (His.Bind System, Novagen) containing a protease inhibitor mixture (Complete Mini, EDTA-free, Roche Molecular Biochemicals) and DNase A. Soluble proteins were recovered by centrifugation at 15000*g* for 15 min. Cell fragments were frozen and submitted two more times to protein extraction. All protein-containing supernatants were pooled and applied to the His.Bind(Ni^{2+} resin) equilibrated column, and proteins were purified as recommended by Novagen. Purified proteins were washed and concentrated with 50 mM potassium phosphate, pH 5.8, by ultrafiltration on a Microcon column (Amicon-Millipore) to a final volume of about 0.5 mL. Selective labeling of the [β-^{13}C]cysteines was achieved as previously described (*19*).

Ahp1 overoxidation was achieved in vitro in 0.5 mL of 50 mM potassium phosphate buffer at 4 °C during 48 h. Ahp1 (0.6 mM) was first reduced by 37 mM DTT (60 equiv). Oxidant *t*BuOOH was then added to a final concentration of 37 mM (60 equiv). After the incubation, the protein was washed by ultrafiltration with 50 mM potassium phosphate buffer, pH 5.8, to obtain 0.5 mL of solution. Free cysteinesulfinic acid and free cysteinesulfonic acid (cysteic acid) (both from Sigma) were dissolved separately in 50 mM Na_3PO_4 (Prolabo) until the pH was 7; the final concentrations in free amino acid were 100 and 75 mM, respectively. The NMR samples were prepared as described below.

NMR Spectroscopy. NMR samples contained ∼1 mM uniformly ^{15}N-, ^{15}N/^{13}C-, or ^{15}N/^{13}C/50% ^{2}H-labeled Ahp1 and ∼0.7 mM selectively [β-^{13}C]Cys-labeled Ahp1, in NMR buffer (50 mM potassium phosphate, 90% H_2O/10% D_2O, 5 mM DTT, 0.02% NaN_3) at pH 5.8. NMR data were collected at 38 °C. One-, two-, and three-dimensional NMR experiments were recorded on Bruker Avance DRX-500 (Lyon) and Varian Inova Unity+ 600 and 800 (Grenoble) spectrometers. Backbone resonance assignments were obtained from a series of deuterium-decoupled heteronuclear three-dimensional experiments [HNCO, d-HN(CA)CO, d-HNCA, d-MQ-HNCOCA, d-HN(CA)CB, d-HN(COCA)CB, d-(H)C(CCO)NH-TOCSY] taken from the Varian Protein Pack, except for the d-MQ-HNCOCA (*20*) and the d-HN(COCA)CB experiments. A 3D ^{1}H−^{15}N NOESY−HSQC experiment (*21*) was recorded with a mixing time of 120 ms. Two-dimensional ^{1}H−^{13}C HSQC and 1D {^{1}H}-decoupled ^{13}C spectra were recorded on the selectively [β-^{13}C]-Cys-labeled samples. The parameters used for the experiments are given in the Supporting Information (Table S1). Quadrature detection in the indirectly detected dimensions was achieved by either echo/antiecho (*22*) or states (*23*) methods. All ^{1}H dimensions were referenced to the H_2O signal relative to DSS, and ^{13}C and ^{15}N dimensions were referenced indirectly using the ^{1}H/X frequency ratios of the zero point (*24*). NMR data were processed and analyzed using NMRPipe (25) and PIPP (26) software packages.

Relaxation Data. All relaxation experiments were performed at 500 MHz at 38 °C. R_1 (longitudinal relaxation rate), R_2 (transverse relaxation rate), and the steady-state ^{1}H−^{15}N NOE measurements were performed using the usual pulse sequences (*27*). The R_1 and R_2 experiments were collected with 130 complex t_1 increments, 1024 t_2 points, and 48 scans for each FID. For R_1 measurements, spectra were recorded with six inversion−recovery delays of 22, 55, 155, 255, 500, and 755 ms and spectra were recorded twice at 155 ms. For R_2 measurements, spectra were recorded at five Carr−Purcell−Meiboom−Gill (CPMG) delays of 17, 33, 50, 67, and 83 ms and spectra were duplicated at 33 and 67 ms. Short delays were used because of fast R_2 rates. A 900 μs period separated two 180° ^{15}N pulses in the CPMG sequence. ^{1}H−^{15}N NOE spectra with 182 × 2 complex t_1 increments, 1024 t_2 points, and 304 scans per FID were recorded in an interleaved way with and without proton saturation during relaxation delay. Recycle delays of 5 and 2 s were used for the spectrum recorded, respectively, in the absence and in the occurrence of proton saturation. The ^{1}H saturation was achieved by the application of 120° ^{1}H pulses separated by 5 ms, for a period of 3 s.

Relaxation Data Analysis. Peak heights (in arbitrary units) of the ^{1}H−^{15}N cross-peaks were measured using PIPP software (*26*). The uncertainty of the peak heights was determined as twice the spectrum noise given by NMRPipe (*25*). The cross-peak heights were then fit to a single-exponential decay function $I(t) = I_0e^{-Rt}$ to get the R_1 and R_2 values ($I(t)$ is the intensity at relaxation delay t, I_0 the intensity at $t = 0$). The errors in R_1 or R_2 were estimated by Monte Carlo simulations. The ^{1}H−^{15}N heteronuclear NOEs were calculated from the ratio between the intensities of a peak in the spectra collected with and without proton saturation, respectively. The errors in the NOE values were determined as standard errors. The Tensor2 software (*28*) was used to obtain the rotational correlation time τ_C.

Hydrogen Exchange Experiments. A solution of [U-^{13}C,^{15}N]-Ahp1 was lyophilized and dissolved in 550 μL of 100% D_2O. A series of ^{1}H−^{15}N HSQC spectra were collected at 38 °C after the addition of D_2O solvent. $H^{N-}N$ cross-peaks that remained observable after more than 20 min were classified as slowly exchanging amide protons.

Analytical Ultracentrifugation. Sedimentation velocity experiments were performed on reduced, overoxidized, and oxidized samples of Ahp1 at 20 and 38 °C. The solvents were the same as in NMR conditions (50 mM potassium phosphate, pH 5.8, 0.02% NaN_3); the reduced and overoxidized samples contained in addition 6 mM DTT. Three protein concentrations were typically investigated (0.8, 5, and 10 mg·mL^{-1}). Samples of 100 or 400 μL were loaded into 3 or 12 mm path length double-sector cells, respectively, and centrifuged at 42000 rpm, using a XL-I analytical ultracentrifuge and an AN-60 TI rotor (Beckman Instruments). The sedimentation profiles were recorded using absorbance optics at 275 nm at typically 5 min intervals and for 11 h. The SEDNTERP program (V 1.01, developed by D. B. Haynes, T. Laue, and J. Philo, available at http://www.bbri.org/RASMB/rasmb.html) was used to calculate, at 38 °C, a solvent density (ρ) and viscosity (η) of 0.9991

$g \cdot mL^{-1}$ and 0.6873 mPa·s, respectively, and a partial specific volume of the protein ($\bar{\nu}$) from the amino acid composition of 0.7383 $mL \cdot g^{-1}$. The corresponding values at 20 °C were 1.0043 $g \cdot mL^{-1}$, 1.0150 mPa·s, and 0.7328 $mL \cdot g^{-1}$. These values were used to normalize the experimental sedimentation (*s*) scale as $s_{20,w}$ values and to estimate theoretical values for the sedimentation coefficients of Ahp1 multimers of globular shape (frictional ratio of 1.25).

The sedimentation profiles corresponding to each sample were analyzed using direct global modeling of the boundary profiles with the program Sedfit (http://www.analyticalultracentrifugation.com/). Sedfit takes advantage of a radial and time-independent noise subtraction (*29*). In a first approach of the program, finite element solutions of the Lamm equation for a large number of discrete, independent species, for which a relationship among mass, sedimentation, and diffusion coefficients is assumed, are combined to represent the experimental data as a continuous size distribution (*30*). We used typically 200 generated sets of data on a grid of 500 radial points, calculated using a frictional ratio of 1.25 for sedimentation coefficients comprised between 2 and 15 or 20 S, at 20 and 38 °C, respectively, to model experimental selected sedimentation profiles (at 20 °C, profiles obtained every 25 min, and at 38 °C, every 10 min, typically) in a continuous distribution of particles, using a regularization procedure (*F* ratio of 0.68) (the details of the procedure are described on the Web site). In a second approach, the sedimentation profiles can be analyzed in terms of one or two noninteracting species, if the model is appropriate (*31*), which allows the independent evaluation of the sedimentation (*s*) and diffusion (*D*) coefficients for each species, from which the molar mass (*M*) is derived using the Svedberg equation: $M = sRT/D(1 - \rho\bar{\nu})$.

Alignment. Peptidic sequences presenting Ahp1 homology were collected with BLAST search on the Swiss-Prot and Tr EMBL protein data banks by NPSA (http://npsa-pbil.ibcp.fr/) (*32*). The criterion of peptidic sequence selection was the presence of the catalytic cysteines and the catalytic conserved residues. Sixty sequences from bacteria, plants, fungi, and animals were aligned with CLUSTALW of NPSA. The Ahp1 sequence (in the upper line) will be the reference for the amino acid numbering given above.

Model Calculation. Models for the monomer of Ahp1 were calculated using Modeller (*33*). The structure of the Prx domain of hybrid Prx5 from *Haemophilus influenzae* (PDB code 1NM3; *34*) was used as a template. The domain presents 32% identity with Ahp1. The NMR data were taken into account for the model calculation and used for the alignment of the peptidic sequences. Constraints were added in Modeller scripts to define the secondary structural elements as defined by NMR data. NOE cross-peaks and hydrogen exchange experiments were used to define the β-strand pairing.

RESULTS

Backbone Assignment. Ahp1 in nonreducing media gave very broad NMR signals that were significantly sharpened in the presence of an excess of DTT. However, the three-dimensional triple-resonance experiments recorded on a [U-^{13}C/^{15}N]-labeled sample of reduced Ahp1 gave poor magnetization transfer. Only 50% of the expected signals could be observed in the HNCA experiment. Ahp1 was then uniformly ^{13}C- and ^{15}N-labeled and 50% uniformly ^{2}H-labeled to yield better spectra. The backbone assignment was accomplished using HNCO, d-HN(CA)CO, d-HNCA, d-MQ-HNCOCA, d-HN(CA)CB, d-HN(COCA)CB, and d-(H)C-(CCO)NH experiments recorded at (^{1}H) 800 and 600 MHz (Supporting Information Table S1). The assignment was also completed and confirmed by sequential NOEs from the ^{15}N NOESY−HSQC experiment. Finally, 92% of the ^{15}N and H^N, 95% of the ^{13}Cα and ^{13}CO, and 90% of the ^{13}Cβ resonances were assigned (BioMagResBank 5816 entry, http://bmrb.wisc.edu/). The $H^{N-15}N$ connectivities of 13 residues (I50, S59, C62, S65, H66, I67, V89, T90, W100, F114, A115, S167, and V169) could not be assigned in the HSQC spectrum. However, 11 unassigned and very weak cross-peaks without any transfer in the triple-resonance experiments remained observable in the HSQC. The ^{13}Cα and ^{13}Cβ resonances of the peroxidatic cysteine C62 and the resolving cysteine C120 have been assigned. C62 resonances could be assigned using interresidual correlations of T63. Strips of the E129−V136 sequence corresponding to the d-HN(COCA)CB and d-HN(CA)CB experiments are shown in Figure 4.

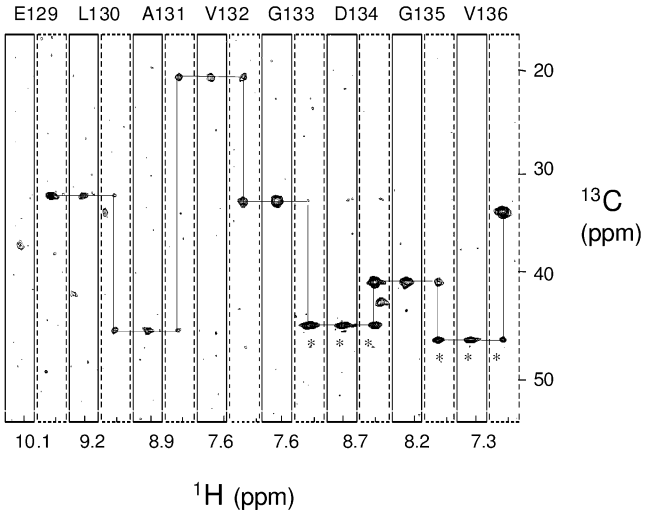

FIGURE 4: ^{1}H/^{13}C strips from distinct ^{15}N planes of the HN(COCA)-CB (continuous line) and HN(CA)CB (dashed line) spectra of reduced [U-^{15}N/^{13}C/50% ^{2}H]Ahp1, giving the ^{13}Cβ sequential connectivities for the E129−V136 sequence. HN(COCA)CB and HN(CA)CB spectra were recorded at 38 °C at 600 and 800 MHz, respectively. ^{1}H and ^{13}C chemical shifts (ppm) are given by the *x* and *y* axes, respectively. Stars indicate glycine ^{13}Cα signals which appear as negative peaks according to the pulse sequence.

Overoxidation. Sulfenic acid RSOH has been shown to be an intermediate in peroxiredoxin mechanisms (Figure 1) (*35*). This sulfenic acid can react readily with another thiol, R′SH, to make a disulfide bond, RS−SR′, which is then reduced by a dithiol. However, a sulfenic acid may also be overoxidized by hydroperoxides into a sulfinate, RSO_2^-, that can be further oxidized into a sulfonate, RSO_3^-. The assignment of the cysteine ^{13}C resonances of Ahp1 enabled us to define the redox state of the cysteine in the inactive Prx overoxidized in vitro by *t*BuOOH. The protein shows the same biochemical properties as the protein characterized after in vivo oxidative stress of Δ*sod1* and Δ*lys7* yeast mutants (*17*). ^{1}H−^{13}C HSQC spectra were recorded for the native reduced protein and for the in vitro overoxidized protein both selectively labeled with [β-^{13}C]Cys (parts A and

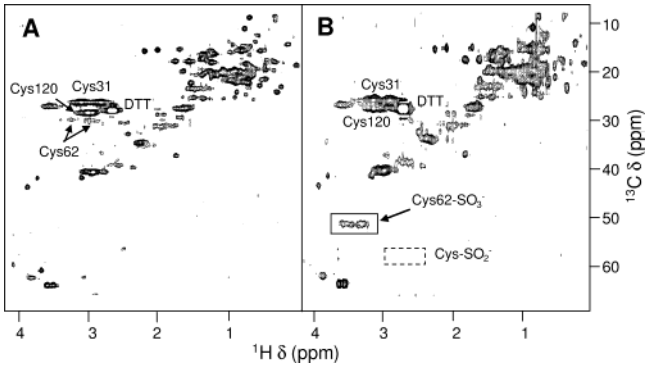

FIGURE 5: $^1H-^{13}C$ HSQC spectra of reduced (A) and overoxidized (B) [β-^{13}C]Cys-labeled Ahp1 recorded at 38 °C and 500 MHz. The additional NMR signals in the HSQC spectra indicate that the [$^{13}C\beta$]-labeled cysteine was metabolized during bacterial growth. The cross-peaks of the three cysteines of Ahp1 are labeled. C62 is the peroxidatic cysteine, and C120 is the resolving cysteine. After the overoxidation, the signals of the peroxidatic cysteine Cys62 are shifted. The positions of the βCH_2 resonances of free cysteine-sulfinate (Cys-SO_2^-) and -sulfonate (Cys-SO_3^-) are schematically indicated by dashed- and solid-lined boxes, respectively.

B of Figure 5, respectively). The spectra are very similar, except for the [β-^{13}C]Cys62 signals. Upon oxidation [β-^{13}C]-Cys62 weak signals ($\delta(^{13}C) = 29.4$ ppm, $\delta(^1H) = 3.30$ and 3.05 ppm) disappear, and a CH_2 system appears at $\delta(^{13}C) = 50.8$ ppm and $\delta(^1H) = 3.50$ and 3.35 ppm (Figure 5). To define the redox state of the cysteine, $^1H-^{13}C$ HSQC spectra of free cysteinesulfinate (Cys-SO_2^-) and -sulfonate (Cys-SO_3^-) were recorded in the same conditions (38 °C, pH 5.8, 50 mM potassium phosphate). References of βCH_2 chemical shifts were obtained: Cys-SO_2^-, $\delta(^{13}C) = 60.1$ ppm, $\delta(^1H) = 2.83$ and 2.71 ppm; Cys-SO_3^-, $\delta(^{13}C) = 52.8$ ppm, $\delta(^1H) = 3.50$ and 3.34 ppm. The observed methylene chemical shifts are therefore in good agreement with the sulfonate chemical shifts ($\Delta\delta(^1H) < 0.1$ ppm, $\Delta\delta(^{13}C) = 1$ ppm), indicating that Ahp1 overoxidized in vitro presents a Cys-SO_3^- residue in the active site.

Topology of Ahp1. The secondary structure of Ahp1 was determined on the basis of $H^{N-1}H$ NOE data, amide proton exchange (*36*), and $^{13}C\alpha$ and ^{13}CO chemical shifts with CSI (*37*) and TALOS (*38*) methods. A summary of the NMR data is given in Figures 6 and 7. Five helices were identified in Ahp1. Helices 3 and 4 start right after proline residues, as commonly observed in many proteins. Three independent β-sheets were characterized. Two antiparallel β-sheets (β1/β2 and β6/β7) are located in the N-terminus and the C-terminus, respectively. A five-stranded mixed parallel and antiparallel β-sheet (β3/β4/β5/β8/β9) folds in a $-1x$, $-1x$, $+3$, $+1$ topology (Figure 7, III). A β-bulge has been characterized at the beginning of β-strand 9. Almost all amide protons of the residues located in the center of the β-sheets are protected from exchange with the solvent (Figure 6). Some amide protons are still observed in the $^1H-^{15}N$ HSQC experiment after several months in D_2O. The hydrogen-bonding in the β-sheets consistent with the observed amide proton exchange and the NOE data is indicated by dashed lines in Figure 7.

^{15}N Relaxation. A uniformly ^{15}N-labeled sample was used to record ^{15}N R_1 and R_2 and $^1H-^{15}N$ NOE relaxation data at 38 °C and (^1H) 500 MHz. The relaxation data are shown in Figure 8. Low $^1H-^{15}N$ NOE values are observed for the N-terminal extremity and for the Q23−K32 segment (A in Figure 8), indicating very flexible regions with fast internal motion. This is in accordance with very few sequential $H^{N-1}H$ NOE correlations being observed for these residues. Another region, V132−V136 (B in Figure 8), exhibits particular dynamic properties, as demonstrated by its clearly higher R_1 values and lower R_2 values, as well as a low $^1H-^{15}N$ NOE for D134. This region would globally remain structured, as suggested by the many sequential and long-range $H^{N-1}H$ NOEs observed. The mean values for the ^{15}N R_1 and R_2 in the regular secondary structure elements are 0.81 ± 0.08 and 19.7 ± 1.9 s^{-1}, respectively. The average R_2/R_1 ratio for these residues allows an estimation of the global correlation time (τ_C) of the protein. A value of 18.4 $\pm$ 0.1 ns was deduced for τ_C using the isotropic model. Further analysis showed that the protein rotational diffusion properties were in fact significantly anisotropic, and a more detailed relaxation interpretation in terms of dynamic parameters therefore required an anisotropic model. Detailed studies of the relaxation data will be published elsewhere.

Analytical Ultracentrifugation. To characterize the dispersion of the oligomeric states of Ahp1, analytical ultracentrifugation experiments were performed at 20 and 38 °C on the oxidized (as extracted from the purification), reduced, and overoxidized forms of Ahp1. Each state was studied at three protein concentrations (0.8, 5, and 10 mg·mL^{-1}). Figure 9 shows the distribution of sedimentation coefficients for the most concentrated samples at 38 °C. Table 1 compares the values of the mean sedimentation coefficient for each

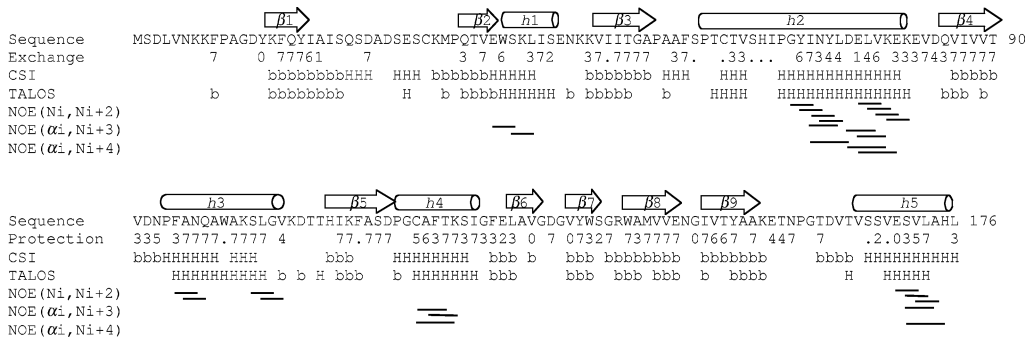

FIGURE 6: Summary of amide exchange data, secondary structures, and patterns of medium-range NOEs for Ahp1. In D_2O exchange of H^N followed by 2D $^1H-^{15}N$ HSQC, residues indexed 0, 1, 2, 3, 4, 5, 6, and 7 give cross-peaks still present after 20 min, 35 min, 1 h, 1.5 h, 3 days, 6 days, 9 days, and 7 months, respectively. Dots are for unassigned residues. In CSI (*37*) and TALOS (*38*) indexes, "H" and "b" represent prediction of helix and β-strand conformations, respectively. Medium-range NOEs characteristic of helices (N*i*, N*i* + 2), (αi, N*i* + 3), and (αi, N*i* + 4) are indicated with lines.

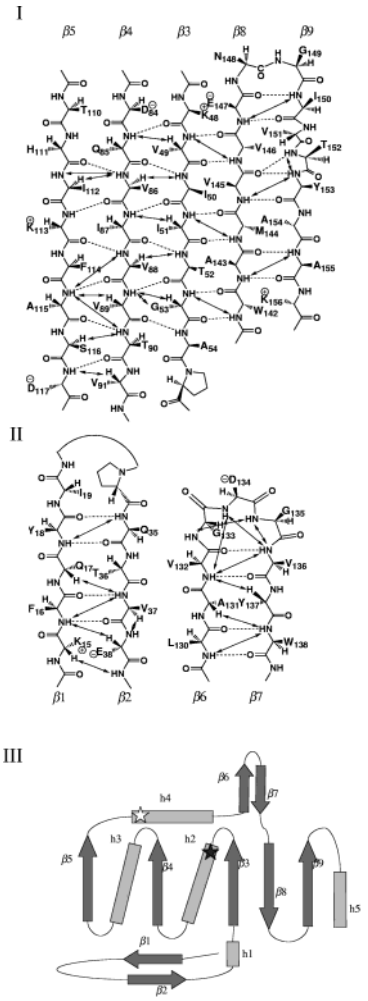

FIGURE 7: β-Strand pairing scheme and topology of Ahp1 deduced from NMR experiments. (I) Central β-sheet composed of parallel (β3/β4/β5) and antiparallel (β3/β8/β9) strands. β-strand 9 presents a β-bulge. Arrows indicate NOE connectivities. (II) Two independent antiparallel β-sheets located next to the N-terminus (β1/β2) and between helix 4 and β-strand 8 (β6/β7). (III) Topology of Ahp1. The peroxidatic cysteine C62 and the resolving cysteine C120 are indicated by a black star in helix 2 and a white star in helix 4, respectively. Secondary structural elements are not displayed to scale.

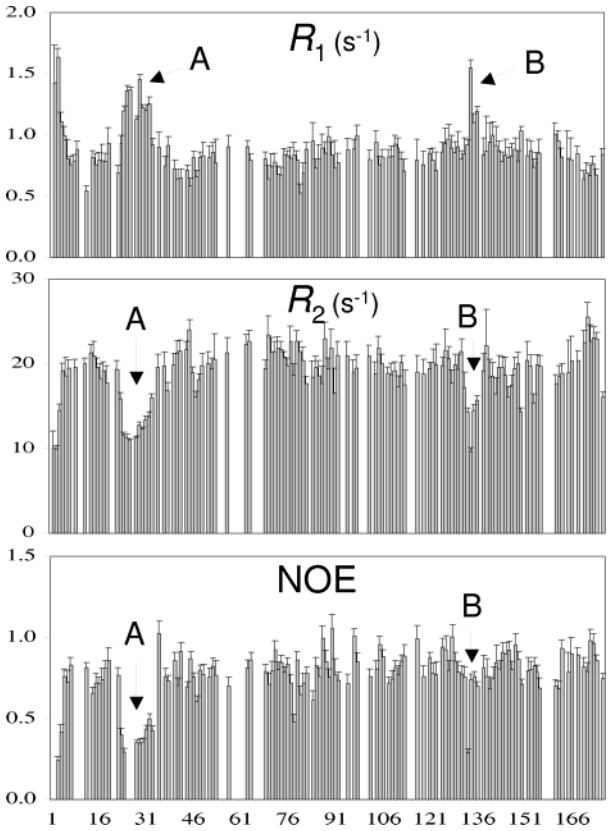

FIGURE 8: ^{15}N relaxation data of Ahp1 recorded at 38 °C and 500 MHz. The relaxation rates R_1 and R_2 and the steady-state heteronuclear NOEs are plotted as a function of the residue number. "A" (Q23−K32) and "B" (V132−V136) indicate two regions of higher mobility (see the text).

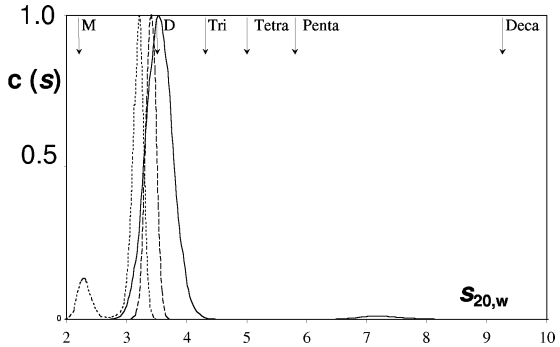

FIGURE 9: Sedimentation velocity experiments of Ahp1. Sedimentation velocity experiments performed at 38 °C and 42000 rpm were analyzed in terms of a continuous distribution of sedimentation coefficients $s_{20,w}$ (see the Experimental Procedures). The vertical scale was adapted to assign for the various samples the same arbitrary concentration for the main sedimenting species. The distributions have been obtained for the 460 μM reduced (dashed line), 460 μM native (oxidized) (continuous line), and 450 μM overoxidized (dotted line) samples. "M", "D", "Tri", "Tetra", "Penta", and "Deca" represent the theoretical $s_{20,w}$ values for the globular monomer, dimer, trimer, tetramer, pentamer, and decamer, respectively.

sample and provides a qualitative characterization of the distribution. The distribution for the reduced sample at 38 °C shows, independently from the protein concentrations, one unique peak with a sedimentation coefficient value ($s_{20,w}$ = 3.4 S) close to that of a theoretical globular dimer (Table 1 and Figure 9). The analysis in terms of noninteracting species leads to a molecular mass range of 42−45 kDa compatible with the dimer (calculated value of 43 kDa). At 20 °C, an autoassociation phenomenon is suggested toward heavier entities (possibly tetramers) from the increase of the mean sedimentation coefficient and the appearance of larger species at the highest concentration (see Table 1). For the native sample, the value of the sedimentation coefficient and the peak width for the main peak increase with the protein concentration (Table 1), showing a clear concentration-dependent autoassociation at 20 °C and, to a lesser extent, at 38 °C.

The behavior of the overoxidized sample is different from that of the other two redox forms. At 38 and 20 °C, the distribution of sedimentation coefficients shows either two peaks at 2.3 and 3.25 S (at 10 mg·mL^{-1}; see Figure 9) or one larger and unresolved peak of maximum 3.15 S (at lower protein concentrations, data not shown). The experimental sedimentation profiles can be correctly fitted by a mixture of 15−25% monomers and 75−85% dimers, without any concentration dependence. The dimer sedimentation coefficient average is slightly smaller (3.2 S) than the native and reduced ones (3.4−3.5 S), while the monomer value (2.3 S)

Table 1: Sedimentation Velocity Experiments of Ahp1

		mean $s_{20,w}$ (S)			
	T (°C)	0.8 mg·mL^{-1} Ahp1	5 mg·mL^{-1} Ahp1	10 mg·mL^{-1} Ahp1	species in addition to the main one at 3−4 S
reduced form	38	3.3	3.4	3.4	
	20	3.3	3.5	3.9	5−8 S at 10 mg·mL^{-1}
oxidized form	38	3.4	3.7	3.9	5−8 S at 5 and 10 mg·mL^{-1}
	20	3.4	3.6	3.8	5−8 S at 0.8, 5, and 10 mg·mL^{-1}
overoxidized form	38	3.0	3.0	3.0	2.2 S at 0.8, 5, and 10 mg·mL^{-1}
	20	3.2		2.9	2.2 S at 0.8 and 10 mg·mL^{-1}

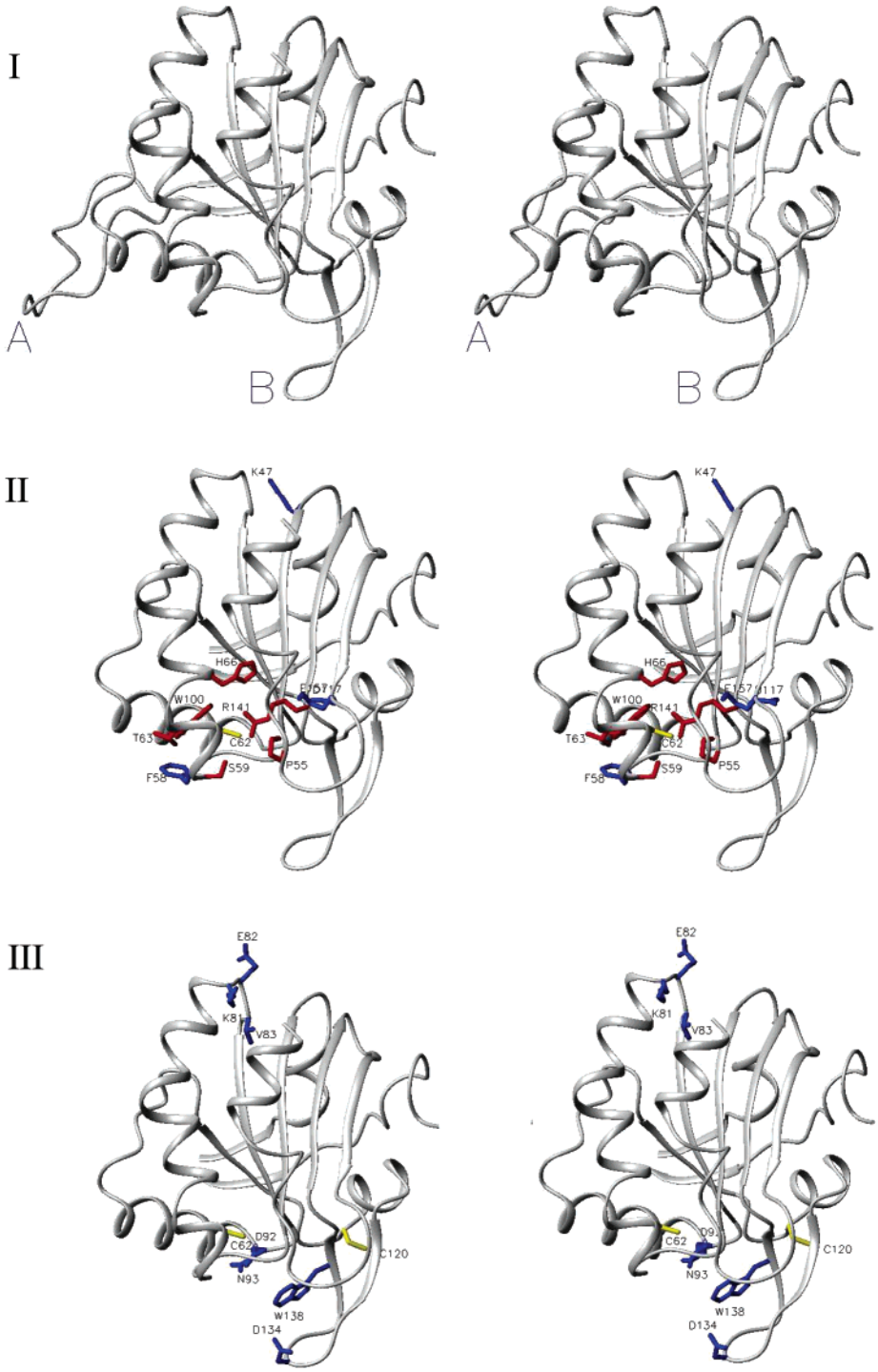

FIGURE 10: Stereoviews of the Ahp1 model. (I) Representation of the backbone of the monomer of Ahp1. "A" and "B" indicate two regions of the protein discussed in the text. (II) Residues conserved in D-type Prx's. For clarity, loop A has been omitted. Residues from the active site of the protein are colored in red. Other conserved residues are colored in blue, and the peroxidatic cysteine C62 is colored in yellow. (III) Ahp1-specific residues (see the text and Figure 3). The peroxidatic and resolving cyteines are both colored in yellow.

is in agreement with the theoretical $s_{20,w}$ (2.2 S) expected for globular species.

DISCUSSION

Structural Characterization of Ahp1. The NMR-based topology of Ahp1 is similar to those of other known Prx structures (reviewed in ref *5*) (Figure 7, III). Models of monomeric Ahp1 were calculated to localize some amino acids as discussed below. For the model calculations, NMR data (NOEs, chemical shifts, and hydrogen exchange experiments) were used to define constraints for the secondary structural elements. The global structure was found to be similar to the structure of D-type Prx's. The thioredoxin fold (β3/h2/β4/h3/h4/β8/β9/h5) is completed by one helix (h1) and five β-strands (β1, β2, β5, β6, β7), β1−β2 and β6−β7 forming two independent β-sheets as illustrated in Figure 10.

Oligomerization of Ahp1. From ^{15}N relaxation data, the correlation time τ_c of reduced Ahp1 was estimated to 18.4 ± 0.1 ns, a value hardly compatible with a monomeric molecular mass of 19 kDa. As a comparison, τ_c values of proteins with molecular mass in the range of 17−18 kDa were calculated from ^{15}N relaxation data at 37 °C (*39*). The τ_C values range between 5.92 and 8.45 ns, with an average value of 7.22 ± 0.56 ns. The τ_c value of Ahp1 strongly suggests that the protein is mainly a stable dimer in solution. This dimeric state in solution is clearly confirmed by sedimentation velocity analysis (Figure 9). Whatever the redox state of the protein, Ahp1 essentially appears as a dimer at 38 °C. Unlike the reduced A-type Prx's (*40*, *41*), no decamers are clearly detected. However, a concentration-dependent autoassociation is observed in the case of the oxidized form. The D-type human PrxV was already suggested to exist as a dimer in its native state according to HPLC gel filtration analysis (*9*) and X-ray crystallography (*34*). For the D-type hybrid Prx5, ultracentrifugation and crystallographic data have shown that the protein is a tetramer, in which both glutaredoxin and Prx domains are dimeric to form a supramolecular enzymatic assembly (*34*). All these results strongly suggest that all D-type Prx's are dimers in solution.

Local Dynamics of Ahp1. According to the ^{15}N relaxation data, two loop regions labeled A and B in Figures 3, 8, and 10 show particular dynamics. These regions are the 10-residue insertion connecting β-strand 1 and β-strand 2 and a turn located between β-strand 6 and β-strand 7, respectively. The loop A (Q23−K32 in Ahp1) is only present in D-type Prx's from some fungi (Figure 3). The insertion is rich in polar residues (S, D/E) and presents one conserved cysteine (Figure 3), but the Cys → Ser mutation does not affect the antioxidant properties of Ahp1 (*1*). All NMR data (chemical shifts, homonuclear NOEs, and relaxation data) indicate that the Q23−K32 loop is unstructured with characteristic fast motions (Figures 6 and 8). This mobile loop is clearly not part of the core structure of the protein (Figure 10, I). This charged loop could potentially be an interaction motif for a biological partner of Prx, such as thioredoxin, glutaredoxin, or another protein. Interestingly, the other mobile loop, V132−V136 (B in Figure 8), is located in a region which presents variable structures in known X-ray crystallographic Prx structures: α-helix (*42*), β-hairpin (*34*, *40*, *41*), or a noncanonical structure (*8*, *43*). According to the NMR data, this region is clearly structured in a β-strand/turn/β-strand conformation in Ahp1 (Figures 6 and 7). NOEs and heteronuclear relaxation data suggest that both the N-terminal insertion and the V132−V136 turn are exposed to the solvent as illustrated in the model (Figure 10, I).

Six residues from the active site (S59, C62, S65, H66, I67, and W100) could not be assigned in the HSQC spectrum, most probably due to broad resonances. This could be caused by specific chemical or conformational exchange at intermediate rates, as recently observed for the active site of the malate synthase G from *E. coli* (*44*). In some X-ray structures of B-type Prx's, the unwinding of helix 2 has been observed (*41*, *45*). Moreover *B* factors of the bacterial Prx AhpC indicate that the active site pocket presents a certain disorder (*6*, *7*). Such a disorder could reflect a flexibility of the redox-active loop necessary for the disulfide formation between distant cysteines.

Overoxidation of Ahp1. Recent in vivo studies have shown that human A-type Prx's are inactivated by overoxidation of the peroxidatic cysteine into sulfinate and/or sulfonate (*6*, *7*, *16*, *46*). Similar effects have been noticed in vitro for mammal, plant, and yeast A-type Prx's (*6*). Bacterial Prx homologues need higher concentrations of hydroperoxide to be inactivated and have a lower sensitivity to overoxidation. The sensitivity of eukaryotic A-type Prx's toward overoxidation is supposed to be associated with structural elements localized mainly in the C-terminal portion (*6*). The corresponding structural elements are found neither in D-type enzymes nor in B-, C-, and E-type Prx's. However, the p*I* and the catalytic properties of Ahp1 have been shown to be affected by overoxidation effects (*17*). We used the specific NMR chemical shifts to determine the redox state of the catalytic cysteine after *t*BuOOH-induced overoxidation. Under the in vitro experimental conditions, the catalytic cysteine appears unambiguously transformed into sulfonate (RSO_3^-) (see Figure 5). Interestingly, analytical ultracentrifugation indicates that the overoxidized form of Ahp1 is slightly different from the oxidized and reduced forms. A monomeric form is detected, constituting 15−25% of the total overoxidized protein sample, whereas oxidized and reduced forms do not appear as monomers. Moreover, the dimer *s* value is slightly, but significantly, lower than the other forms. This could indicate a possible loss of compactness of the overoxidized dimer.

Residues Conserved in the D-Type Prx's. Eleven residues are invariable, or nearly invariable, within 60 sequences of D-type Prx's, a selection of which is given in Figure 3 for clarity. These conserved residues correspond to K47, P55, F58, S59, C62, T63, H66, W100, D117, R141, and E157 in the Ahp1 protein (in bold in Figure 3). P55, S[T]59, C62, and R141 residues are also found in all other Prx's as shown in Figure 2. Six residues (P55, S59, T63, H66, W100, and R141) (in red in Figure 10, II) are part of the active site surrounding the peroxidatic C62 (in yellow). P55 protects C62 from solvent accessibility (*6*). R141 is proposed to stabilize the anionic form of C62 and probably lowers its pK_a value (*47*−*49*). The hydroxylated residue homologous to S59 in other D-type Prx's (threonine) is thought to play an activating role on the peroxidatic cysteine as the proton acceptor of the Cys62 Hγ (*50*). The residue threonine forms a hydrogen bond with the cysteine in all reduced Prx structures. The Ahp1 Ser → Asp mutant inactivity supports

such a role for this residue (*17*). In B- and D-type Prx X-ray structures (*8*, *34*, *42*), the tryptophan homologous to W100 forms a hydrogen bond with the conserved hydroxylated residue homologous to T63. This bond constrains the bulky side chain of W100 to obstruct one side of the active site. H66 located near R141 obstructs another side of the active site. The four other invariant residues, K47, F58, D117, and E157, are displayed in blue in Figure 10, II. K47 is located near the surface opposite the active site. No particular role is described for this charged residue. F58 is conserved in all Prx's except C- and E-types. This hydrophobic residue is involved in the dimer−dimer interface of the A-type Prx's (*45*). The charged residue D117 forms a hydrogen bond with the backbone amide of the hydrophobic residue $i + 5$ (F122) localized at the beginning of helix 4. This bond stabilizes and could orient helix 4. Next to β-strand 9, the anionic residue E/D (E157 in Ahp1) makes hydrogen bonds with the backbone of residues of the loop preceding helix 5.

Other residues are conserved in more than 80% of the 60 D-type Prx sequences. A number of conserved hydrophobic residues are indicated in Figure 3. In all the D-type Prx's but Ahp1, the turn between helix 2 and β-strand 4 is characterized by the dipeptide G[V/I/A]. The dipeptide is replaced in Ahp1 by the sequence K81E82V83, which provides charged residues at the surface of the protein, opposite the active site (Figure 10, III). In the so-called B region of D-type Prx's (Figures 3 and 10, I), a hydrophobic residue is found in a conserved tripeptide, G[F/L/M]G. The hydrophobic residue is replaced in Ahp1 by a charged residue (D134), which gives a negative charge in the turn between β-strand 6 and β-strand 7 (Figure 10, III). Other residues are conserved in all D-type Prx's but Ahp1 (in gray in Figure 3). These conserved residues are the polar and charged residues ND located in the turn between β-strand 4 and helix 3 and R located at the end of β-strand 7 (in gray in Figure 3). In Ahp1, the arginine is replaced by a tryptophan (W138) and the dipeptide ND by DN (D92N93) (Figure 10, III). The last particularity of the Ahp1 sequence is the resolving C120. A homologous cysteine is found only in the sequence of MLF3_MALFU, a Prx from the yeast *Mallassezia furfur* (Figure 3). According to SDS−PAGE gels, this Prx also forms an intermolecular disulfide in the oxidized state of the enzyme (*18*). In the other D-type Prx's, the resolving cysteine C120 is replaced by a Gly in 50% of the sequences or by Ala or Leu in the other sequences.

D-Type Prx Homodimer Interface. Structural analysis of the human PrxV and *H. influenzae* hybrid Prx5 dimers (*34*) shows that the D-type Prx interface is mainly stabilized by hydrophobic interactions, through residues homologous to F58, S59, P60, and F95 in Ahp1 (Figure 3). Other residues involved in the interface are conserved in all D-type Prx's but Ahp1 (F120, R133, and D79). The residue F120 of human PrxV and *H. influenzae* hybrid Prx5 is replaced in Ahp1 by the anionic residue D134 (Figures 3 and 10, III). The residues R133 and D79 that form an intermolecular salt bridge in hybrid Prx5 (*34*) are replaced by neutral residues (W138 and N93) in Ahp1 (Figures 3 and 10, III). Therefore, the homodimer interface of Ahp1, which should involve residues located around the peroxidatic and the resolving cysteines (Figure 10, III), cannot be unequivocally deduced. Further studies will be undertaken to define the dimer interface of Ahp1.

ACKNOWLEDGMENT

We thank Dr. Jean-Pierre Simorre, Dr. Bernhard Brutscher, and Yannick Pelletier from the Institut de Biologie Structurale Jean-Pierre Ebel, Grenoble, France, for their technical support.

SUPPORTING INFORMATION AVAILABLE

Tables S1, NMR experiments and parameters used to acquire chemical shift assignments of Ahp1, and S2, peptidic sequence alignment of 60 D-type peroxiredoxins from fungi, bacteria, archaebacteria, and animals. This material is available free of charge via the Internet at http://pubs.acs.org.

REFERENCES

1. Jeong, J. S., Kwon, S. J., Kang, S. W., Rhee, S. G., and Kim, K. (1999) *Biochemistry 38*, 776−783.
2. Lee, J., Spector, D., Godon, C., Labarre, J., and Toledano, M. B. (1999) *J. Biol. Chem. 274*, 4537−4544.
3. Verdoucq, L., Vignols, F., Jacquot, J.-P., Chartier, Y., and Meyer, Y. (1999) *J. Biol. Chem. 274*, 19714−19722.
4. Park, S. G., Cha, M.-K., Jeong, W., and Kim, I.-H. (2000) *J. Biol. Chem. 275*, 5723−5732.
5. Wood, Z. A., Schröder, E., Harris, J. R., and Poole, L. B. (2003) *Trends Biochem. Sci. 28*, 32−40.
6. Wood, Z. A., Poole, L. B., and Karplus, P. A. (2003) *Science 300*, 650−653.
7. Woo, H. A., Chae, H. Z., Hwang, S. C., Yang, K.-S., Kang, S. W., Kim., K., and Rhee, S. G. (2003) *Science 300*, 653−656.
8. Choi, H.-J., Kang, S. W., Yang, C.-H., Rhee, S. G., and Ryu, S.-E. (1998) *Nat. Struct. Biol. 5*, 400−406.
9. Seo, M. S., Kang, S. W., Kim, K., Baines, I. C., Lee, T. H., and Rhee, S. G. (2000) *J. Biol. Chem. 275*, 20346−20354.
10. Horling, F., König, J., and Dietz, K.-J. (2002) *Plant Physiol. Biochem. 40*, 491−499.
11. Dietz, K.-J. (2003) *Annu. Rev. Plant Biol. 54*, 93−107.
12. Kong, W., Shiota, S., Shi, Y., Nakayama, H., and Nakayama, K. (2000) *Biochem. J. 351*, 107−114.
13. Baker, L. M. S., and Poole, L. B. (2003) *J. Biol. Chem. 278*, 9203−9211.
14. Rouhier, N., Gelhaye, E., and Jacquot, J.-P. (2002) *J. Biol. Chem. 277*, 13609−13614.
15. Choi, J., Choi, S., Choi, J., Cha, M.-K., Kim, I.-H., and Shin, W. (2003) (in press).
16. Rabilloud, T., Heller, M., Gasnier, F., Luche, S., Rey, C., Aebersold, R., Benahmed, M., Lousot, P., and Lunardi, J. (2002) *J. Biol. Chem. 277*, 19396−19401.
17. Prouzet-Mauléon, V., Monribot-Espagne, C., Boucherie, H., Lagniel, G., Lopez, S., Labarre, J., Garin, J., and Lauquin, G. J.-M. (2002) *J. Biol. Chem. 277*, 4823−4830.
18. Yasueda, H., Hashida-Okado, T., Saito, A., Uchida, K., Kuroda, M., Onishi, Y., Takahashi, K., Yamaguchi, H., Takesako, K., and Akayama, K. (1998) *Biochem. Biophys. Res. Commun. 248*, 240−244.
19. Krimm, I., Lemaire, S., Ruelland, E., Miginiac-Maslow, M., Jacquot, J.-P., Hirasawa, M., Knaff, D. B., and Lancelin, J.-M. (1998) *Eur. J. Biochem. 255*, 185−195.
20. Brutscher, B., Cordier, F., Simorre, J.-P., Caffrey, M. S., and Marion, D. (1995) *J. Biomol. NMR 5*, 202−206.
21. Schleucher, J., Schweiendinger, M., Sattler, M., Schmidt, P., Schedletsky, O., Glaser, S. J., Sørensen, O. W., and Griesinger, C. (1994) *J. Biomol. NMR 4*, 301−306.
22. Cavanagh, J., and Rance, M. (1990) *J. Magn. Reson. 88*, 72−85.
23. States, D. J., Haberkorn, R. A., and Ruben, D. J. (1982) *J. Magn. Reson. 48*, 286−292.
24. Wishart, D. S., Bigam, C. G., Yao, J., Abildgaard, F., Dyson, H. J., Oldfield, E., Markley, J. L., and Sykes, B. D. (1995) *J. Biomol. NMR 6*, 135−140.
25. Delaglio, F., Grzesiek, S., Vuister, G. W., Zhu, G., Pfeifer, J., and Bax, A. (1995) *J. Biomol. NMR 6*, 277−93.
26. Garrett, D. S., Powers, R., Gronenborn, A. M., and Clore, G. M (1991) *J. Magn. Reson., Ser. B 95*, 214−220.

27. Farrow, N. A., Muhandiram, R., Singer, A. U., Pascal, S. M., Kay, C. M., Gish, G., Shoelson, S. E., Pawson, T., Forman-Kay, J. D., and Kay, L. E. (1994) *Biochemistry 33*, 5984−6003.
28. Dosset, P., Hus, J.-C., Blackledge, M., and Marion, D. (2000) *J. Biomol. NMR 16*, 23−28.
29. Schuck, P., and Demeler, B. (1999) *Biophys. J. 76*, 2288−2296.
30. Schuck, P. (2000) *Biophys. J. 78*, 1606−1619.
31. Schuck, P. (1998) *Biophys. J. 75*, 1503−1512.
32. Combet, C., Blanchet, C., Geourjon, C., and Deléage, G. (2000) *Trends Biochem. Sci. 25*, 147−150.
33. Sali, A., Potterton, L., Yuan, F., van Vlijmen, H., and Karplus, M. (1995) *Proteins 23*, 318−26.
34. Kim, S. J., Woo, J. R., Hwang, Y. S., Jeong, D. G., Shin, D. H., Kim, K., and Ryu, S. E. (2003) *J. Biol. Chem. 278*, 10790−10798.
35. Ellis, H. R., and Poole, L. B. (1997) *Biochemistry 36*, 15013−15018.
36. Wüthrich, K. (1986) *NMR of proteins and nucleic acids* Wiley, New York.
37. Wishart, D. S., Sykes, B. D., and Richards, F. M. (1992) *Biochemistry 31*, 1647−1651.
38. Cornilescu, G., Delaglio, F., and Bax, A. (1999) *J. Biomol. NMR 13*, 289−302.
39. Åkerud, T., Thulin, E., Van Etten, R. L., and Akke, M. (2002) *J. Mol. Biol. 322*, 137−152.
40. Wood, Z. A., Poole, L. B., Hantgan, R. R., and Karplus, P. A. (2002) *Biochemistry 41*, 5493−5504.
41. Schröder, E., Littlechild, J. A., Lebedev, A. A., Erringhton, N., Vagin, A. A., and Isupov, M. N. (2000) *Structure 8*, 605−615.
42. Declercq, J.-P., Evrard, C., Clippe, A., Vander Stricht, D., Bernard, A., and Knoops, B. (2001) *J. Mol. Biol. 311*, 751−759.
43. Hirotsu, S., Abe, Y., Okada, K., Nagahara, N., Hori, H., Nishino, T., and Hakoshima, T. (1999) *Proc. Natl. Acad. Sci. U.S.A. 96*, 12333−12338.
44. Tugarinov, V., Muhandiram, R., Ayed, A., and Kay, L. E. (2002) *J. Am. Chem. Soc. 124*, 10025−10035.
45. Alphey, M. S., Bond, C. S., Tetaud, E., Fairlamb, A. H., and Hunter, W. N. (2000) *J. Mol. Biol. 300*, 903−916.
46. Wagner, E., Luche, S., Penna, L., Chevallet, M., van Dorsselaer, A., Leize-Wagner, E., and Rabilloud, T. (2002) *Biochem. J. 366*, 777−785.
47. König, J., Lotte, K., Plessow, R., Brockhinke, A., Baier, M., and Dietz, K.-J. (2003) *J. Biol. Chem. 278*, 24409−24420.
48. Montemartini, M., Kalisz, H. M., Hecht, H.-J., Steinert, P., and Flohé, L. (1999) *Eur. J. Biochem. 264*, 516−524.
49. Bryk, R., Griffin, P., and Nathan, C. (2000) *Nature 407*, 211−215.
50. Flohé, L., Budde, H., Bruns, K., Castro, H., Clos, J., Hofmann, B., Kansal-Kalavar, S., Krumme, D., Menge, U., Plank-Schumacher, K., Sztajer, H., Wissing, J., Wylegalla, C., and Hecht, H.-J. (2002) *Arch. Biochem. Biophys. 397*, 324−335.

BI035551R